tron. Mater., **8**, 249 (1979).

17a. W. v. Münch, W. Kurzinger, and I. Pfaffender, *Solid State Electron.*, **19**, 871 (1976).
17b. W. v. Münch and W. Kurzinger, *ibid.*, **21**, 1129 (1978).
17c. W. v. Münch, *J. Electron. Mater.*, **6**, 449 (1977).
18. W. v. Münch, Private communication.
19. W. v. Münch and I. Pfaffender, *This Journal*, **122**, 642 (1975).
20. W. v. Münch and I. Pfaffender, *J. Appl. Phys.*, **48**, 4831 (1977).
21. G. K. Safaraliev, Yu. M. Tairov, V. F. Tsvetkov, and Yu. Kriger, *Sov. Phys. Semicond.*, **10**, 226 (1976).
22. Y. M. Tairov and V. F. Tsvetkov, in "Progress in Crystal Growth and Characterization," Vol. 7, P. Krishan,

Editor, p. 111, Pergamon Press, New York (1983).
23. H. Matsunami, S. Nishino, and H. Ono, *IEEE Trans. Electron. Dev.*, **ed-28**, 1235 (1981).
24. S. Nishino, J. A. Powell, and H. A. Will, *Appl. Phys. Lett.*, **42**, 460 (1983).
25. A. Addamiano and J. A. Sprague, *ibid.*, **44**, 525 (1984).
26. L. H. Blake and E. Mendel, *Solid-State Technol.*, **42** (1970).
27. A. I. Kingon, L. J. Lutz, P. Liaw, and R. F. Davis, *J. Am. Ceram. Soc.*, **66**, 558 (1983).
28. P. Liaw and R. F. Davis, *This Journal*, **131**, 634 (1984).
29. J. Graul and E. Wagner, *Appl. Phys.*, **21**, 67 (1972).
30. C. J. Mogab and H. J. Leamy, *J. Appl. Phys.*, **45**, 1075 (1974).

Transient Behavior during Film Removal in Diffusion-Controlled Plasma Etching

Richard C. Alkire* and Demetre J. Economou**

Department of Chemical Engineering, University of Illinois, Urbana, Illinois 61801

ABSTRACT

A mathematical model is formulated to analyze transient behavior during film removal from closely spaced wafers in a barrel plasma etching reactor. The model incorporates diffusion and simultaneous reactions which include the etching process as well as recombination reactions of both volume and surface types. The analysis relates the effect of geometric and operating variables to process characteristics such as etch uniformity, over-etch exposure, and throughput. Dimensionless system parameters are identified and are used to express computed results in general form. Regions of operating conditions that permit etch uniformity within specified tolerances are found, and optimum settings for inter-wafer spacing and reactor pressure to achieve maximum throughput are calculated.

Important goals for plasma processing include yield, throughput, and uniformity. Variables which are commonly controlled to achieve these goals include reactor geometry, design and operating conditions, choice of chemicals introduced into the plasma, and adjustment of wafer position within the reaction zone. It is the nature of such complex systems that engineering trade-offs exist in identifying "optimum" settings. Often, however, a seemingly minor adjustment in a sensitive variable can cause a major change in performance. Also, it is invariably difficult to translate successful experience with one system to a new system on the basis of intuition alone. For these reasons, purely empirical programs of development can be time consuming.

Mathematical methods have been used to model a wide variety of chemical reactor systems, and have been found useful in guiding development strategies for improvement. In the present study, a mathematical model was developed to predict transient behavior during film removal from closely spaced wafers in a barrel etcher.

The barrel plasma etching reactor, shown schematically in Fig. 1, consists of a cylindrical quartz chamber that has input gas manifolds and a vacuum pumping outlet. RF power, commonly at 13.56 MHz, is coupled to the reactor through external electrodes and an impedance matching network. The wafers are loaded on a boat in a stand-up configuration with the wafer axes along the barrel axis. In order to achieve high throughput, the interwafer spacing is made small so that the reactor may hold dozens of wafers in a single batch. During operation, gas is continuously introduced into the reactor. Active species, which are generated by electron-impact dissociation in the plasma region, diffuse in the interwafer space and react with the film on the wafer surface. At the same time, the active species may degrade by recombination reactions within the reactor volume or on the walls. Since etching is solely due to neutral species, the resulting edge-profile exhibits mask "undercut" characteristic of isotropic etching. Hence, the barrel etcher cannot be used for etching

fine line geometries. Sometimes an Al perforated cylinder is placed coaxially around the wafers. With the "etch tunnel" present, the plasma is confined in the annular region between the metal cylinder and the reactor wall; active species have then to diffuse through the perforations and, since the diffusion path is lengthened, the etch rate is smaller with the etch tunnel.

Stripping of photoresist in an oxygen plasma in a barrel-type reactor was the first application of plasma etching in semiconductor processing (1). Etching of Si, poly-Si, and Si_3N_4 in fluorine containing plasmas (especially in CF_4/O_2 mixtures) quickly found widespread applications (2). Similar reactors are also used for LPCVD processes (4, 18).

Etch uniformity and throughput are of particular importance in any plasma etching process. Across-wafer and wafer-to-wafer uniformity are both critical in etching patterned films since local loading can rapidly enhance mask undercut after the end point has been reached. Parameters that affect uniformity and throughput include RF power input, chamber pressure, gas flow rate and distribution, wafer spacing, wafer diameter, and tem-
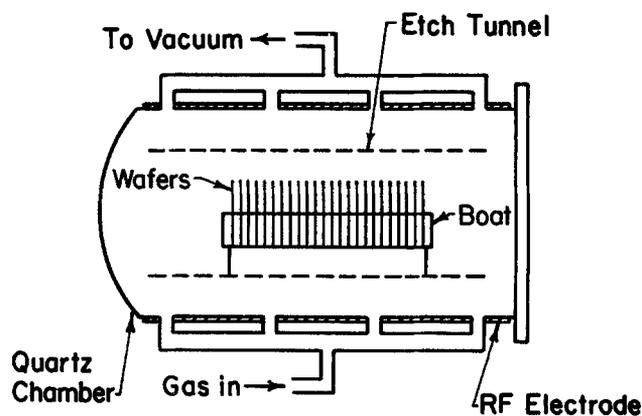

Fig. 1. Schematic of a barrel plasma etching reactor

perature. Several investigators have reported models for diffusion-controlled plasma etching in barrel reactors (5, 6). With assumption of steady-state conditions, the effect of process parameters on etch uniformity was studied.

In the present work, transient removal of a film from a wafer stacked in a barrel plasma etcher is investigated. Transport and reaction phenomena are used to predict behavior and to identify dimensionless scale-up parameters. This study differs from past work in that transient behavior is included so that the duration of etch cycle (throughput) and of over-etch exposure may be investigated. While actual plasma systems are more complex, the following model provides a basic framework which may be expanded as additional refinements are added.

Theoretical Formulation

Let us for the moment concentrate on events happening in the interwafer space, regarding the gas discharge outside the wafer stack as simply the source of etchant species. The plasma region is treated later. Figure 2, not drawn to scale, is a schematic representation of the radially symmetric cell formed by two wafers facing each other. Prior to the onset of etching, a film of uniform thickness exists on the wafer surfaces. The rate of film removal depends on the concentration distribution in the interwafer gap. To an extent that depends upon operating conditions, the etch rate is highest on the periphery of the wafer. Film in this region thus clears first, and subsequent film removal would then take place in more inaccessible regions. Figure 2 illustrates the situation part way through the process, where film has been cleared entirely from the outer portion of the wafer, while the inner region is yet to clear. As etching proceeds, the concentration distribution changes to conform to the reactivity distribution along the wafer surface. While the film may eventually be removed everywhere, the peripheral regions would meanwhile be exposed to overetching conditions which, in many systems, adversely affect product quality.

The following assumptions preserve the salient features of the system and also streamline the task of computation. 1. The spacing between adjacent wafers is sufficiently smaller than the wafer radius so that significant concentration variations occur only in the radial direction. 2. Convection is negligible with respect to diffusion


Fig. 2. Schematic of the radially symmetric region between two successive wafers.

in the interwafer region owing to the large value of the diffusion coefficient. An order of magnitude calculation showed that, even if all the gas were flowing parallel to the wafer surfaces, the Pe number ($=R_0u_g/D$) would be less than 0.05. In practical systems, with the gas outlet at the back of the quartz barrel, most of the gas flow is normal to the wafer surfaces. Thus, practical Pe numbers are even smaller. 3. The etching reaction is first order; this has been shown for photoresist stripping in oxygen (6) and Si etching in fluorine (7). 4. The etching reaction proceeds to completion at or near the film surface (6) over a distance much smaller than the diffusion length of the etching species, and the reaction products do not affect the etching process (8). 5. The substrate is not etched. Hence the model is applicable to processes such as photoresist stripping in an O_2 plasma or Si etching in a CF_4/O_2 plasma with SiO_2 as the substrate. 6. The pressure remains constant during an etch cycle; this can be achieved by using a pressure feed-back control system. 7. Operation is isothermal with no spatial variations of diffusivity or reaction rate constants. This assumption will not be valid in cases of highly exothermic etching reactions. For example, in etching Si at 0.5 μm/min in a F containing plasma, the adiabatic temperature rise of a 10 cm diam 0.5 mm thick slice will be 1.3°C/s. Furthermore, severe temperature variations will occur during start-up, unless a preheat-treatment with a N_2 or Ar plasma is applied. 8. The concentration of etchant at the wafer edge remains constant during the etch cycle. However, if the etching reaction is the main loss mechanism for the etchant species, and the reaction rate distribution along the wafer surface is nonuniform, the etchant concentration at the wafer edge (c_0) will change with time during a single etch cycle. This is because the amount of film remaining on the wafers will also change with time (loading effect). Such a change in c_0 could be predicted by Eq. [19] to be derived later. The calculations presented in this work did not account for any changes in c_0 during an etch cycle (see also "Conclusions" section). 9. The concentration profiles adjust rapidly to the gradual movement of the film front during depletion. Therefore, at any particular moment, the concentration distribution is at the steady-state distribution which corresponds to the reactivity conditions prevailing at that moment. This "pseudo-steady-state" approximation is valid provided that the time scale over which film depletion occurs (equal to $\chi h_0/k_2c_0$, see also expression for τ in Eq. [5]) is much greater than the "characteristic" diffusion time (R_0^2/D). In other words, the following inequality should hold: $\chi h_0D/k_2c_0R_0^2 \gg 1$. For typical values of the parameters (Table I), this ratio is found to be greater than 10^3.

During etching, the thickness of etchable material left at a certain location and time will be given by

$$h(r,t) = h_0 - \int_0^t \frac{k_2}{\chi} c(r,t)\, dt \qquad [1]$$

The concentration distribution $c(r,t)$ varies with time during the etching process and is calculated by application of transport laws to the movement of etchant species. The remaining text in this section consists of three segments: the general model, a limiting case valid in the absence of recombination reactions, and a method for determining the concentration of etching species at the edge of the wafer stack.

General model.—Under the foregoing assumptions stated above, the conservation equation for the etching species is

$$D\frac{1}{r}\frac{d}{dr}\left(r\frac{dc}{dr}\right) = \frac{2k_2}{L}c + 2k_1c^2[A_2] + \frac{v_0w}{2L}c \qquad [2]$$

with the boundary conditions

$$c = c_0 \text{ at } r = R_0$$

$$\frac{dc}{dr} = 0 \text{ at } r = 0$$
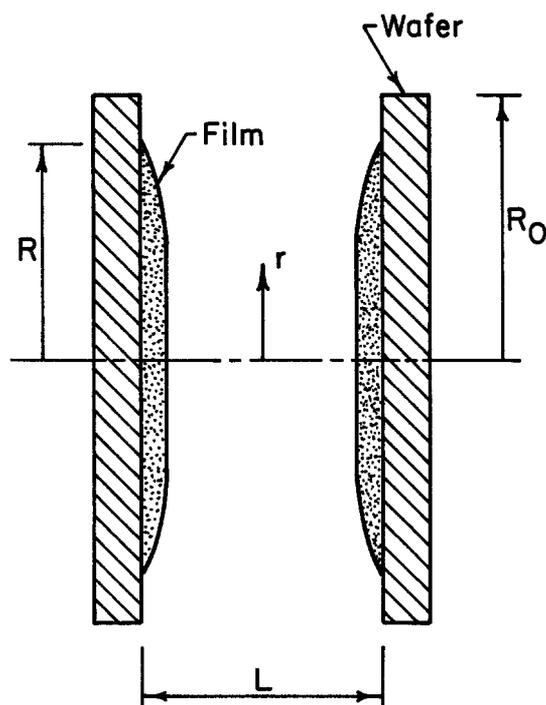
The left-hand side of Eq. [2] represents the radial diffusion of etchant into the region between the wafers, while the right-hand side (rhs) corresponds to the various reactions which occur. The first term on the rhs of Eq. [2] represents etching. Since only radial concentration gradients are assumed to exist, the heterogeneous reaction rate k_2c is transformed to a homogeneous rate term by multiplication by the surface to volume ratio $2/L$. Both surfaces have been assumed reactive, *i.e.*, the wafers stand back to back during etching. When etching patterned films, this term has to be multiplied by the fraction of the surface occupied by etchable material. Note that $k_2 = 0$ for $r > R$, where the film no longer exists (Fig. 2). The second term on the rhs of Eq. [2] represents volume recombination reactions of the active species of the form

$$A + A + A_2 \xrightarrow{k_1} 2A_2 \qquad [3]$$

A_2 is the parent molecule which gives A, the etching species, by electron-impact dissociation. A_2 acts as a third body for recombination to occur. The presence of a third body is required to conserve momentum and energy during recombination. The reverse of reaction [3] proceeds at negligibly small rates at the low temperatures used in plasma etching [*e.g.*, the equilibrium constant for the reaction $F_2 \rightleftarrows 2F$ is $\approx 10^{-24}$ mol/cm³ at 300 K (19)]. When the concentration of the etching products is low, $[A_2] \cong P/R_gT$ $- [A] = P/R_gT - c$. The third term on the rhs of Eq. [2] accounts for wall recombination of the active species in reactions of the form

$$A + (A * \text{wall}) \xrightarrow{w} A_2 + \text{wall} \qquad [4]$$
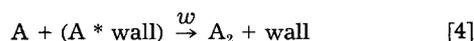
This term results by multiplying the random flux of etchant striking the wafer surface $(1/4 \, v_oc)$ by the surface to volume ratio $(2/L)$ and by the wall recombination coefficient w, which is assumed constant throughout the wafer surface. The wall recombination reaction is first order since an impinging atom recombines with an atom already adsorbed on the surface (9).

Before proceeding further, it is convenient to rewrite the governing equations in terms of dimensionless quantities based on the following definitions

$$\zeta = \frac{r}{R_o} \qquad H = \frac{h}{h_o}$$

$$\qquad \qquad \qquad \qquad \qquad \qquad [5]$$

$$C = \frac{c}{c_o} \qquad \tau = \frac{k_2c_o}{\chi h_o} t$$

When the variables defined in Eq. [5] are introduced into Eq. [1] and [2], the following dimensionless equations arise

$$H = 1 - \int_0^\tau C d\tau \qquad [6]$$

$$\frac{d^2C}{d\zeta^2} + \frac{1}{\zeta} \frac{dC}{d\zeta} = \phi_o{}^2C + \alpha C^3 + \beta C^2 + \gamma C \qquad [7]$$

with

$$\alpha = -\frac{2k_1R_o{}^2c_o{}^2}{D} \qquad \gamma = \frac{v_owR_o{}^2}{2LD}$$

$$\qquad \qquad \qquad \qquad \qquad \qquad [8]$$

$$\beta = \frac{2k_1PR_o{}^2c_o}{(R_gT)D} \qquad \phi_o{}^2 = R_o{}^2 \frac{2k_2}{LD}$$

The dimensionless boundary conditions become

$$C = 1 \text{ at } \zeta = 1$$

$$\frac{dC}{d\zeta} = 0 \text{ at } \zeta = 0$$

Dimensionless number ϕ_o is comparable to the Thiele Modulus found in catalytic reactor design (17); ϕ_o represents the relative importance of the kinetics of etching as

compared to diffusion. If $\phi_o \gg 1$, for example, diffusion is the controlling step, and one may expect concentration gradients to develop in the interwafer space and the etch rate distribution to be nonuniform. Under such conditions, the outer edge of the wafer would be exposed to overetching, while the center is yet to clear. If $\phi_o \ll 1$, the etching reaction is sluggish and the reaction rate distribution is uniform all over the reacting surface.

Dimensionless groupings α and β describe volume recombination *vs.* diffusion effects. For example, if $\beta \gg 1$, the reactive species recombine before they have any chance to diffuse and etch the wafer surface. Volume recombination reactions are strongly dependent on pressure. For instance, α and β increase with the third power of pressure. Notice that since the partial pressure of the etching species is usually less than 10% of the reactor total pressure, $|\alpha| \leq 0.1\beta$. Finally, grouping γ describes surface recombination *vs.* diffusion effects and is affected by both the surface to volume ratio and the wall recombination coefficient. The latter depends critically on the nature and the condition of the surface.

By solving Eq. [6] and [7], the effect of process parameters $(c_o, P, D, k's)$ and of geometric factors (L, R_o) on etch uniformity, overetch exposure, and total etch time can be determined. In particular, optimum conditions for high throughput can be identified. The above model extends previous studies by accounting for both volume and surface recombination reactions. In addition, the model includes transient effects owing to the pseudo-steady-state clearing of the film.

Note that Eq. [7] is general enough to handle more complex recombination reaction schemes. An example concerning an oxygen plasma is given in the Appendix.

The solution to Eq. [6] and [7] was obtained in a stepwise manner. The wafer was divided in a number of concentric rings of equal width. At each time step, the concentration profile was found by linearizing Eq. [7] about a trial solution and casting the linearized equation into finite difference form by using the central difference approximation. The resulting tridiagonal system was inverted in a CDC Cyber 175. Calculations started about the trial solution obtained analytically when all reaction terms are assumed to be first order in concentration. After the true concentration profile was found, the time required to completely strip the outer ring was determined, and a new film thickness distribution was computed by using Eq. [6]. A new concentration profile was then determined for which the wafer surface was reactive everywhere except for the ring already etched away. With the revised concentration distribution, the time necessary to completely strip the second ring was found. In a like manner, the time needed to strip each successive ring was calculated. The total etch time was the sum of the partial times. For each time step but the first, the solution found in the previous time step was used as the trial solution. No convergence problems were experienced for the values of the parameters used. Results did not differ appreciably by changing the number of rings from 150 to 200. Results were checked against the analytic solution for the limiting case of no recombination reactions discussed below.

Limiting case: no recombination reactions.—When recombination reactions can be neglected ($k_1 = w = 0$), *i.e.*, when the etchant has a long lifetime in the absence of etchable material, Eq. [2] can be simplified into the following two equations

$$D \frac{1}{r} \frac{d}{dr} \left(r \frac{dc}{dr} \right) = \frac{2k_2c}{L} \qquad [9]$$

for $0 \leq r \leq R$, *i.e.*, for the region still occupied by the film, and

$$r \frac{dc}{dr} = \text{const.} \qquad [10]$$

for $R \leq r \leq R_o$, *i.e.*, for the film-free region near the periphery of the wafer.

It is convenient to introduce the following dimensionless variables

$$\psi = \frac{r}{R}, \quad C = \frac{c}{c_o}, \quad \text{and} \quad \phi^2 = R^2 \frac{2k_2}{LD}$$

The film radius R (and not the wafer radius R_o) was used in these definitions so that, although R is changing, the value of ψ is pinned at 1 for $r = R$. The dimensionless form of Eq. [9] is

$$\frac{d^2C}{d\psi^2} + \frac{1}{\psi}\frac{dC}{d\psi} = \phi^2 C \tag{11}$$

which is a Bessel equation. The boundary conditions are

$$C = C_R \text{ at } \psi = 1$$

$$\frac{dC}{d\psi} = 0 \text{ at } \psi = 0 \tag{12}$$

The dimensionless form of Eq. [10] is

$$\zeta \frac{dC}{d\zeta} = \text{const.}$$

with $\zeta = r/R_o$ as before in the general model. The pertinent boundary conditions are

$$C = 1 \text{ at } \zeta = 1$$

$$C = C_R \text{ at } \zeta = \frac{R}{R_o} = \sigma$$

C_R is eliminated by requiring the flux to be continuous at $r = R$. The final result for the concentration distribution is

$$C = \frac{I_o(\phi\psi)}{I_o(\phi) - \phi I_1(\phi) \ln \sigma} \qquad 0 \leq r \leq R \tag{13}$$

$$C = 1 + \frac{\phi I_1(\phi) \ln \zeta}{I_o(\phi) - \phi I_1(\phi) \ln \sigma} \qquad R \leq r \leq R_o \tag{14}$$

where

$$I_o(x) = \sum_{n=0}^{\infty} \frac{(x/2)^{2n}}{(n!)^2}$$

is the modified Bessel function of the first kind of order zero and

$$I_1(x) = \sum_{n=0}^{\infty} \frac{(x/2)^{2n+1}}{n!(n + 1)!}$$

is the modified Bessel function of the first kind of order one. Since $R = R(t)$, Eq. [13] and [14] have a time dependence built into the equations.

The overall etch rate at any given time is

$$2\pi R_o LD \frac{dc}{dr}\bigg|_{r=R_o} = 2\pi LDc_o \frac{\phi I_1(\phi)}{I_o(\phi) - \phi I_1(\phi) \ln \sigma}$$

If the concentration of the etchant were c_o throughout the wafer surface, the etch rate would be

$$2k_2 c_o(\pi R^2)$$

Thus, the "effectiveness factor" η is

$$\eta = \frac{2\pi R_o LD \dfrac{dc}{dr}\bigg|_{r=R_o}}{2k_2 c_o \pi R^2} = \frac{2I_1(\phi)}{\phi[I_o(\phi) - \phi I_1(\phi) \ln \sigma]} \tag{15}$$

The effectiveness factor is an expression of the actual overall reaction rate as compared to the reaction rate that would be obtained if the concentration were at the bulk value throughout the reacting surface (17). A more general expression for the effectiveness factor is

$$\eta = \frac{2 \displaystyle\int_0^R re(c)dr}{R^2 e(c_o)} \tag{16}$$

When the reaction rate is first order in concentration, $e = k_2 c$, Eq. [16] becomes

$$\eta = \frac{2 \displaystyle\int_0^R rc\,dr}{R^2 c_o} = 2 \int_0^1 \psi C d\psi \tag{17}$$

The effectiveness factor concept is used below for the prediction of the etchant concentration in the plasma space surrounding the wafer rack.

The analysis up to this point has concentrated on events occurring in between the wafers. A similar analysis can be applied to LPCVD processes. The recent work by Meyerson and Olbricht (24) is quite relevant. Up to this point, the plasma existing outside the wafer stack has been regarded as simply the source of etchant species. The only parameter, related to the plasma region, that is required for the solution of Eq. [6] and [7] is the etchant concentration at the edge of the wafer stack, c_o. This quantity depends on a complex way on reactor geometry and operating parameters such as power, pressure, flow rate, etc. Prediction of c_o would be less difficult for "clean" systems involving a single gas. An example of such a system is photoresist stripping in an O_2 plasma. The procedures for evaluating c_o are given below.

Etchant concentration in the plasma.—The bulk etchant concentration (c_o) can be predicted by writing a conservation equation for the etchant species (10, 20). These species are generated by electron-impact dissociation of the parent molecules and are eliminated by recombination reactions (Eq. [3] and [4]), etching, and gas flow. Rapid backmixing tends to eliminate concentration gradients in the annular region outside the wafer rack where the plasma exists, particularly when the gas is symmetrically fed through manifolds parallel to the barrel axis. A conservative order of magnitude calculation gave a value for the Pe number less than 0.1. Thus, complete mixing can be assumed in that region (continuous stirred tank reactor model, CSTR). The species balance equation will then read

$$2k_e <n_e> [A_2] V_p = \eta k_2 c_o (N\pi R^2)$$

$$+ \frac{v_o w}{4} S_p c_o + 2k_1 c_o^2 [A_2] V_p + Fc_o \tag{18}$$

The term on the left-hand side of Eq. [18] represents production of etchant species via the reaction

$$A_2 + e \xrightarrow{k_e} 2A + e$$
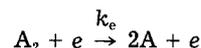
The electron density has been assumed constant at the average value within the annular plasma space. This may be a good approximation if the thickness of the annular space is small compared to its length. Thus, the assumption is better if an etch tunnel is present. In addition, if the principal loss of electrons is a volume process (e.g., attachment), the electron density will tend to be uniform irrespective of the geometry.

The first term on the right-hand side of Eq. [18] represents loss of etchant in the etching reaction. This term depends on the number of wafers (N) and on the area of etchable material left on each wafer (πR^2). The last term in Eq. [18] represents etchant loss by flow. Under the assumption that the gas is essentially composed of A_2 and A (i.e., low loading of wafers), $[A_2] \simeq P/R_g T - c_o$. Then, Eq. [18] gives

$$- c_o^3 + \frac{P}{R_g T} c_o^2$$

$$+ \frac{\dfrac{\eta k_2 \pi R^2 N}{V_p} + \dfrac{v_o w}{4a} + \dfrac{F}{V_p} + 2k_e <n_e>}{2k_1} c_o$$

$$- \frac{k_e <n_e> P}{k_1(R_g T)} = 0 \tag{19}$$

The solution to the cubic Eq. [19] provides c_0. Note that since both R and η are functions of time, c_0 will be time dependent except in the case $\eta k_2 \pi R^2 N/V_p << v_0 w/4a$ or F/V_p or $2k_e <n_e>$. Neglecting the volume recombination reaction $(k_1 \cong o)$ results

$$c_0 \cong \frac{2k_e <n_e> \left(\dfrac{P}{R_g T}\right)}{\dfrac{\eta k_2 \pi R^2 N}{V_p} + \dfrac{v_0 w}{4a} + \dfrac{F}{V_p} + 2k_e <n_e>}$$ [20]

This equation correctly predicts the loading effect in that a plot of $1/c_0$ vs. N results in a straight line (10).

Both the average electron density $<n_e>$ and the dissociation reaction rate constant k_e depend on pressure. In particular, k_e depends on the E_e/P ratio which is a unique function of the electron temperature. In general, determination of $<n_e>$ or k_e is an extremely difficult task. The presence of "hot" electrons, the multiplicity of the reaction channels, and the large number of chemical species involved make the problem of analyzing a gas discharge a very complicated one. The papers by Kushner (21, 22) illustrate the complexity of the problem. A rigorous analysis of the discharge requires knowledge of cross-sectional data for the various collisional processes occurring. Such data are scarce for most of the plasmas used in practice. However, the situation is less complicated when dealing with discharges of a single gas. For the O_2 discharge, in particular, the required physical data are available and a reasonably accurate analysis of an O_2 plasma can be realized. For such a discharge, the effective electric field-to-pressure ratio E_e/P as well as the average electron density $<n_e>$ can be evaluated for given pressure, power density, and reactor geometry from Fig. 1.19 of Ref. (11). After finding the E_e/P ratio, k_e can be obtained from Fig. 1.26 of the same reference. Then c_0 can be computed by using Eq. [20] or the more complicated Eq. [19], if necessary. Hence, the effect of reactor pressure and power input on the bulk etchant concentration can be evaluated for this particular discharge. The plots in Fig. 1.19 and 1.26 of Ref. (11) can be used for analyzing etching in an O_2 plasma as long as the byproducts of etching (CO_2, CO, H_2O, etc.) are in low enough concentrations not to alter the discharge properties. Measurement of $<n_e>$ is usually done with Langmuir probes and is associated with certain experimental difficulties (23). The etchant concentration can be measured by optical emission spectroscopy (12) or by gas-phase titration (13, 14).

Results and Discussion

The foregoing model was employed to predict across-wafer uniformity, etch cycle duration, optimum throughput, and overetch exposure.

Consider first the situation where recombination reactions are negligible, and where steady-state concentration profiles have become established but film clearing has not yet begun. Such a situation corresponds to the simple limiting case described by Eq. [13] with $\sigma = 1$. Figure 3 illustrates how the concentration distribution in the interwafer region depends upon the Thiele Modulus (ϕ_0). For values of ϕ_0 less than 0.3, the concentration distribution (and thus the etching rate distribution) is nearly uniform. That is, the wafer surface is uniformly accessible to the etchant species. For a given wafer diameter and reactor pressure, small ϕ_0 values can be achieved by increasing the wafer spacing, although such action serves also to decrease the throughput. For high ϕ_0 values, diffusion is sluggish compared to the etching reaction so that etching species become depleted from the interwafer region and large radial concentration gradients build up. This will be the case when the wafer spacing is small, or the diffusivity is low (i.e., pressure is high), or the etching reaction is rapid.

A plot of the effectiveness factor η vs. the Thiele Modulus ϕ_0 (Eq. [15]) for two values of the dimensionless film radius $\sigma (= R/R_0)$ is shown in Fig. 4. When $\phi = \phi_0 \sigma << 1$ (i.e., $\phi < 0.1$), Eq. [15] reduces to
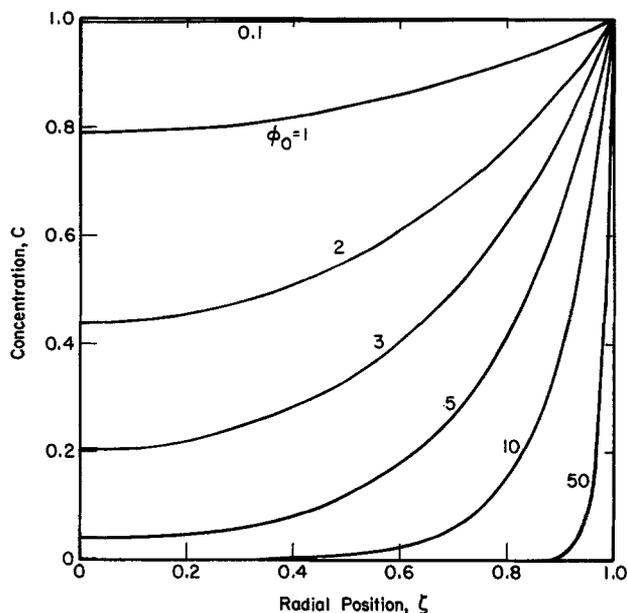

Fig. 3. Effect of Thiele Modulus ϕ_0 on the concentration distribution in the interwafer region prior to film depletion ($\sigma = 1$, $\alpha = \beta = \gamma = 0$).

$$\eta = \frac{4}{4 + \phi_0^2 \sigma^2 (1-2 \ln \sigma)}$$ [21]

For any value of σ, the effectiveness factor tends to unity for small values of the Thiele Modulus ϕ_0. This agrees with the fact that for small ϕ_0 the concentration is at its bulk value (c_0) throughout the wafer surface (e.g., Fig. 3 with $\phi_0 = 0.1$).

When $\phi >> 1$ (i.e., $\phi > 10$), Eq. [15] reduces to

$$\eta = \frac{2}{\phi_0 \sigma (1-\phi_0 \sigma \ln \sigma)}$$ [22]

Before film depletion sets in, $R = R_0$ or $\sigma = 1$. Then Eq. [22] becomes

$$\eta = \frac{2}{\phi_0}$$ [23]

and a log-log plot of η vs. ϕ_0 will result in a straight line with a slope of -1. (Fig. 4 for $\sigma = 1$.)

For any film radius R less than the wafer radius R_0, ($\sigma < 1$), and for high enough values of the Thiele Modulus ϕ_0 so that $-\phi_0 \sigma \ln \sigma >> 1$, Eq. [22] becomes

$$\eta = - \frac{2}{\phi_0^2 \sigma^2 \ln \sigma}$$ [24]

and a log-lot plot of η vs. ϕ_0 will result in a straight line with slope of -2. (Fig. 4 for $\sigma = 0.2$.)

Figure 5 depicts the concentration distribution in the interwafer space for several values of, in essence, the vol-
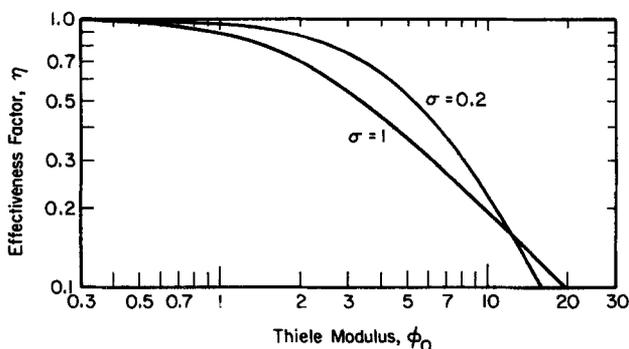

Fig. 4. Effectiveness factor η as a function of the Thiele Modulus ϕ_0 with the dimensionless film radius σ as a parameter (Eq. [15]).
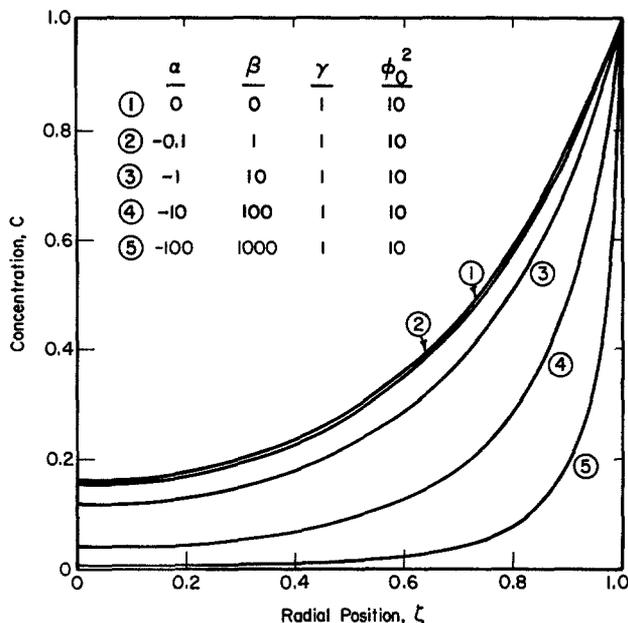
Fig. 5. Effect of volume recombination reactions on the concentration distribution in the interwafer space prior to film depletion (σ = 1).

Fig. 7. Concentration distribution in the interwafer space at different cumulative etch times τ (parameter values are the same as in Fig. 6).

ume recombination reaction rate constant k_1. As k_1 increases so that $|\alpha| >> 1$ and $\beta >> 1$, strong concentration gradients develop which result in a highly nonuniform etch rate and a longer etch time. That is, reactants recombine to inactive species before they can diffuse into the wafer stack and etch the film. However, if k_1 is low enough so that $\beta < 1$, volume recombination reactions can be completely neglected (compare cases ① and ② in Fig. 5). This is true for the commonly employed O_2 or/and CF_4 discharges at pressures less than 1 torr. However, it may not be true for Cl_2 discharges, where the volume recombination rates are faster.

Figure 6 shows the film thickness distribution during transient film clearing with the dimensionless time as a parameter. Initially, the film has a uniform thickness h_0 ($H = 1$). After a dimensionless time of 1, the film begins to recede from the periphery. For this particular example, the film will be completely cleared after a dimensionless time of 10.1 has elapsed. The intersects with the ordinate provide the film radius R as a function of time.

Figure 7 shows the time dependence of the concentration profile during transient clearing of the film. After the outer rings have been cleared, the reactant penetrates more readily to the inner portion of the wafer and thus the concentration increases with time at a given radial position. This increase is less pronounced close to the center of the wafer since this region stays reactive almost throughout the cycle. Figure 6 gives the film thickness distribution as a function of time under the same conditions.

Exposure to overetch is to be avoided in etching most patterned films since local loading can result in rapid mask undercut after the end point has been reached. The percent overetch exposure as a function of the Thiele Modulus ϕ_0 is shown in Fig. 8 for four different radial positions on the wafer surface ζ ($=r/R_0$). In constructing Fig. 8, only surface (not volume) recombination reactions have been included ($\alpha = \beta = 0$, $\gamma = 1$). The percent overetch was computed by

$$\% \text{ overetch} = \frac{\tau_0 - \tau}{\tau} \times 100$$

where τ_0 is the total etch time (shown in the insert Table in Fig. 8), and τ is the time required to clear the film up to a given radial position ζ. Since the portion of the wafer closer to the periphery clears first, the overetch exposure is higher for larger ζ values. Furthermore, as the Thiele Modulus ϕ_0 increases, the radial distribution of the reaction rate becomes nonuniform, resulting in an increase of the overetch exposure.

A related plot is shown in Fig. 9, where the total etch time τ_0 has been plotted against the Thiele Modulus ϕ_0

Table I. Typical parameter values for barrel plasma etchers

| Parameter value	Comments
$[A_2] = 6 \times 10^{-8}$ mol/cm^3	Parent gas partial pressure of 1 torr
$c_0 = 6 \times 10^{-9}$ mol/cm^3	Etchant partial pressure of 0.1 torr
$D \approx 350$ cm^2/s	Estimated for O in O_2 at 400 K and 1 torr. Varies as P^{-1} and approximately at $T^{1.5}$
$h_0 = 10^{-4}$ cm (1 μm)	—
$k_1 \approx 10^{15}$ cm^6/(mol)^2/s	Corresponds to the reaction O + O + $O_2 \rightarrow 2\,O_2$ (11)
$k_2 \approx 50$ cm/s	Calculated from the value of k_2/D = 0.158 cm^{-1} given by Battey (6) It would correspond to an etch rate of 0.55 μ/min for Si in F at c_0 given above
$L_r = 1$ cm	Reference interwafer spacing
$P_r = 1$ torr	Reference reactor pressure
$Q = 100$ sccm	Corresponds to 1850 cm^3/s at 400 K and 1 torr
$R_0 = 5$ cm	—
$T = 400$ K	—
$v_0 \approx 7 \times 10^4$ cm/s	Thermal velocity of O at 400 K
$w = 3 \times 10^{-4}$	For O recombining on silica at 400 K (9) very sensitive to surface conditions
$\chi = 0.33$	Corresponds to the reaction Si + 4F → SiF^4

Fig. 6. Film thickness distribution at different cumulative etch times τ ($\alpha = -1$, $\beta = 10$, $\gamma = 0$, $\phi_0^2 = 25$ and total etch time $\tau_0 = 10.1$).

$\alpha = \beta = 0, \; \gamma = 1$	
ϕ_0	τ_0
0.1	1.27
0.5	1.33
1	1.53
2	2.33
3	3.65
5	7.86
10	27.3
20	103
50	587
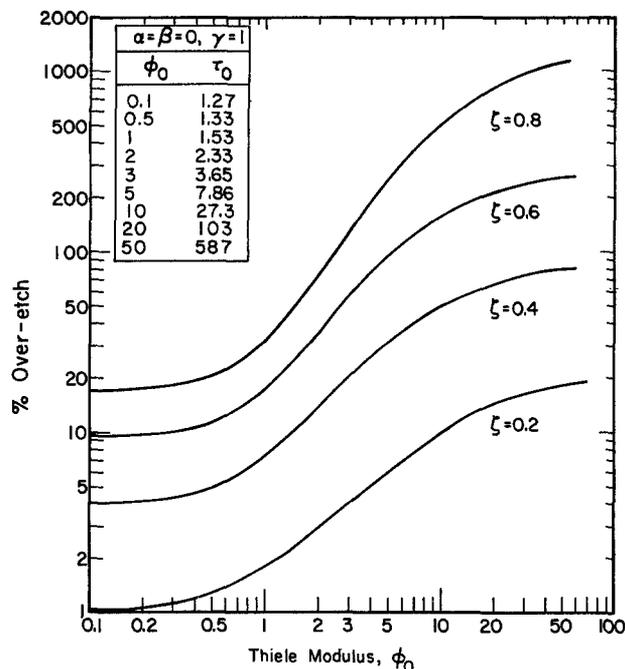
Fig. 8. Overetch exposure (%) vs. Thiele Modulus ϕ_0 for different radial positions on the wafer surface ζ ($\alpha = \beta = 0$, $\gamma = 1$).

with the surface recombination number γ as a parameter. No volume recombination reactions are considered. Since the edge of the wafer clears at a time $\tau = 1$, the percent maximum overetch will be $(\tau_0 - 1) \times 100$ and is also shown on the vertical axis. From Fig. 9, we observe that for $\gamma < 0.1$ and $\phi_0 < 0.3$ the film clears uniformly, *i.e.*, there is no overetch exposure. As one expects, etch time and overetch increase as γ or/and ϕ_0 increase. In addition, for a particular value of γ, the corresponding curve approaches asymptotes for $\phi_0 \ll 1$ and $\phi_0 \gg 1$.

The effect of wafer spacing on throughput is illustrated in Fig. 10, where $1/L^*\tau_0$ (multiplied by 100) has been plotted against the dimensionless wafer spacing L^*. If the wafer thickness and the turnaround time are neglected, $1/L^*\tau_0$ is proportional to the throughput. The curve has been constructed by assigning a value of 5 to $\phi_0{}^2$ and a value of 1 to γ for a dimensionless wafer spacing of $L^* =$
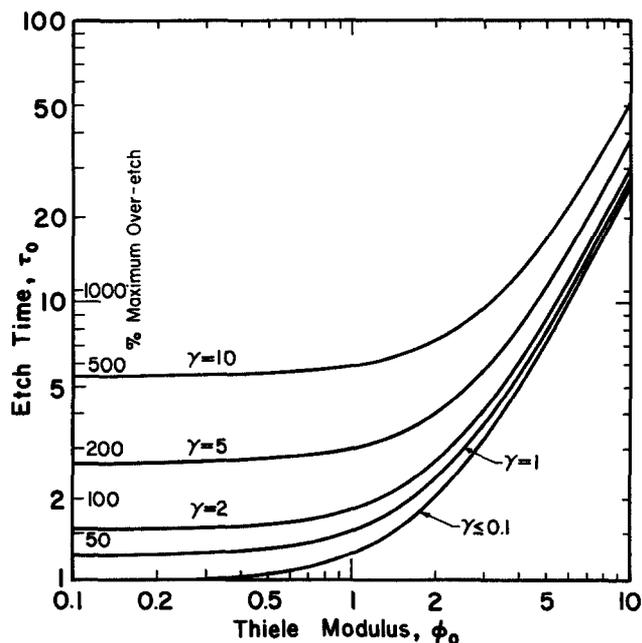

Fig. 9. Total etch time τ_0 and maximum overetch exposure (%) vs. Thiele Modulus ϕ_0 with the surface recombination number γ as a parameter ($\alpha = \beta = 0$).
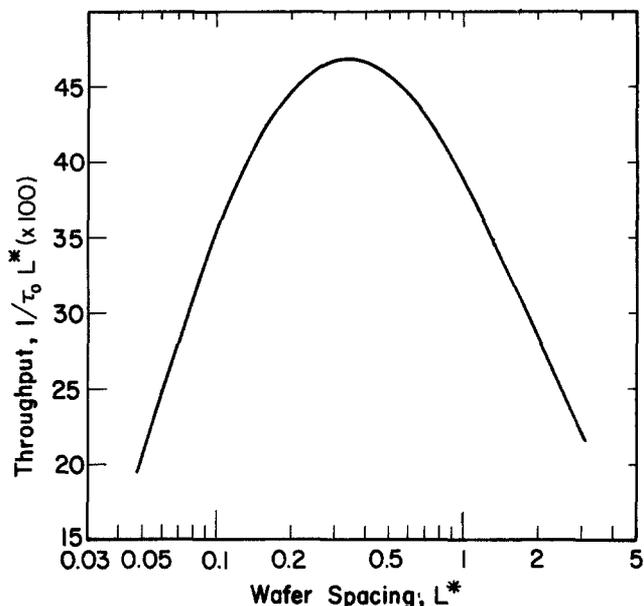

Fig. 10. Effect of wafer spacing on throughput

1. The values chosen for $\phi_0{}^2$ and γ have been calculated by using typical values for the system parameters shown in Table I. By changing the wafer spacing L, γ and $\phi_0{}^2$ change inversely proportionally. No volume recombination reactions have been considered since the corresponding dimensionless groups have no L dependence. The maximum in the plot can be explained as follows. As L^* becomes large, the total etch time $\tau_0 \to 1$ and by further increasing L^* the ratio $1/L^*\tau_0$ decreases. However, as L^* becomes small, τ_0 increases more rapidly, resulting in decreasing throughput $1/L^*\tau_0$. Thus, there is a maximum in the throughput as a function of the wafer spacing. For the parameter values used, this maximum is found from Fig. 10 to occur at $L = 0.4$ cm. This is to be compared with a spacing of 3/16 in. usually employed in stripping photoresists in an O_2 plasma. Direct quantitative comparison with published experiments is difficult since not all of the required system parameters (for example, wall recombination coefficient) are known.

Another parameter affecting the throughput is reactor pressure. Figure 11 depicts the dependence of the total etch time τ_0 on the dimensionless pressure P^*. In constructing Fig. 11, base values of $\alpha = -0.005$, $\beta = 0.05$, $\gamma = 1$, and $\phi_0{}^2 = 5$ have been assigned for a value of pressure $P^* = 1$. Again, the parameter values have been calculated by using Table I. In order to correctly determine the effect of pressure on τ_0, the dependence of the bulk etchant con-
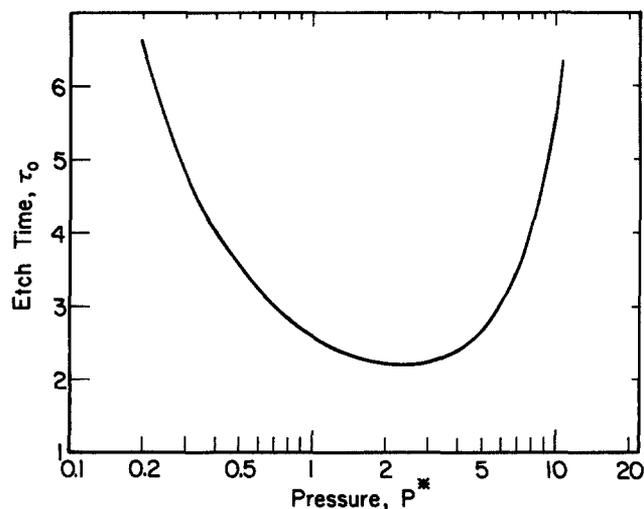

Fig. 11. Effect of reactor pressure on total etch time

centration c_o on pressure must be known. A linear relationship is assumed here (Eq. [20] and Ref. (15) and (16)), so that the dimensionless groups depend on pressure P as follows: $\alpha \sim P^3$, $\beta \sim P^3$, $\gamma \sim P$, $\phi_o^2 \sim p$ (diffusivity $\sim P^{-1}$), and $\tau \sim P$ (since $\tau \sim c_o$). The minimum in the etch time can be explained as follows: at high pressures, the etchant concentration is high but recombination reactions and low diffusivity establish large concentration gradients in the interwafer space. As a result, the etch time increases. However, at low pressures, diffusion is facile and recombination reactions are sluggish but there is not enough etchant species to etch the film. Thus, the strip time is again high. For this particular choice of the parameter values, the minimum in etch time is found from Fig. 11 to occur at about $P^* = 2$ or $P = 2$ torr. Note that $\tau = t/t_o$, where $t_o = (k_2c_o/\chi h_o)^{-1}$ (Eq. [5]) is the "characteristic" etch time equal to 1.85 min for the parameter values of Table I. Hence, the minimum etch time of Fig. 11 would correspond to an etch duration of about 4 min.

The optima shown in Fig. 10 and 11 have been obtained under otherwise no constraints. For example, maximum allowances in overetch exposure are not accounted for. Thus, a pressure of 2 torr (resulting in $\phi_o^2 \sim 10$ for the case considered) would be too high for etching a patterned film.

The present analysis has limitations with respect to the range over which wafer spacing L and pressure P can vary. For example, for wafer spacings comparable to the wafer radius, the one-dimensional model is no longer valid. Furthermore, at low pressure and small wafer spacing, the diffusion mode may be of "Knudsen diffusion" when the mean free path becomes comparable to wafer spacing. This will happen for $PL < 0.05$ torr-cm. Nonetheless, the optimum L and P values are within the range where the model assumptions are valid. For instance, for the optimum wafer spacing of 0.4 cm, the pressure value below which Knudsen diffusion prevails is 0.125 torr. This is far from the optimum pressure value.

Conclusions

A mathematical model for transient clearing of films from restricted geometries has been developed. Dimensionless groupings of system parameters were used to compile behavior and to reveal scale-up principles. The effect of these parameters on etch uniformity, overetch exposure, and throughput was determined, and optima were identified. The model can be extended without much difficulty to handle more complex situations such as: (i) arbitrary etching reaction kinetics, (ii) other types of volume or surface recombination reactions, (iii) nonuniform initial film thickness, (iv) etchable substrate (reaction rate nonuniformities are critical in this case, since the substrate layer may be seriously damaged), (v) time varying bulk concentration (this requires solution of Eq. [19] at each time step after the effectiveness factor has been found from Eq. [15]), and (vi) spatial dependence of the wall recombination coefficient.

The model represents a simplified view by virtue of several assumptions. For example, the wafer temperature may change during etching if the reaction is accompanied by heat effects. Furthermore, the wafer temperature may depend on the reactor pressure. Since chemical reactions are affected by temperature, the reaction rate constant (k_2) may not be a constant. Other assumptions include one-dimensional concentration distribution and pseudo-steady state. Both assumptions can be relaxed, but at the expense of much higher computation time. Finally, detailed analysis of the plasma region is, for the majority of situations, extremely difficult.

Despite its simplicity, the model can serve as a basis for studying more complex systems. An example is removal of polymer drill smear from the holes of multilayer printed-circuit boards (3). Experimental work aimed at testing the model predictions is currently in progress in our laboratory.

Plasma processing systems are complex in the sense that several different phenomena may control overall behavior depending upon the choice of operating conditions. As a consequence, the efficient design and scale-up of plasma systems is usually difficult to accomplish by intuition alone. The use of mathematical models can assist in organizing scientific concepts into strategies for engineering design.

APPENDIX

Recombination Reactions in an Oxygen Plasma

Oxygen plasmas are frequently employed for stripping photoresist masking layers. If the wafer load is small enough so that the stripping products are at negligible concentration, the pertinent recombination reactions will be (11)

$$2\ O + O_2 \xrightarrow{K_1} 2\ O_2$$

$$3\ O \xrightarrow{K_2} O + O_2$$

$$O + 2\ O_2 \xrightarrow{K_3} O_3 + O_2$$

$$O + O \xrightarrow{w} O_2$$
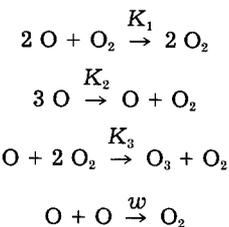
For this system, Eq. [7] will be of exactly the same form but with the dimensionless groupings redefined as follows

$$\alpha = \frac{2(K_2 + K_3 - K_1)R_o^2c_o^2}{D}$$

$$\beta = \frac{2(K_1 - 2K_3)PR_o^2c_o}{(R_gT)D}$$

$$\gamma = \left[\frac{v_ow}{2L} + \frac{2K_3P^2}{(R_gT^2)}\right]\frac{R_o^2}{D}$$

with ϕ_o remaining the same as before.

LIST OF SYMBOLS

a	specific volume of plasma space (V_p/S_p) (cm³/cm²)
A	etchant species
A_2	parent molecule
c_o	etchant concentration at the wafer edge (mol/cm³)
c	etchant concentration (mol/cm³)
C	dimensionless etchant concentration (c/c_o)
c_R	etchant concentration at $r = R$ (mol/cm³)
D	etchant diffusivity (cm²/s)
e	etch rate (mol/cm²/s)
E_e	effective electric field in the plasma region (V/cm)
F	gas volumetric flow rate (cm³/s)
h	film thickness (cm)
h_o	initial film thickness (cm)
H	dimensionless film thickness (h/h_o)
k_1	volume recombination reaction rate constant (cm⁶/(mol)²/s)
k_2	etch rate constant (cm/s)
k_e	electron-impact dissociation rate constant (cm³/mol/s)
L	wafer separation distance (cm)
L_r	reference interwafer spacing (1 cm)
L^*	dimensionless wafer separation distance (L/L_r)
$<n_e>$	average electron density (mol/cm³)
N	number of wafers
P	pressure (torr)
P_r	reference pressure (1 torr)
P^*	dimensionless pressure (P/P_r)
r	radial position (cm)
R	film radius (cm)
R_o	wafer radius (cm)
R_g	gas constant (62,360 torr-cm³/mol/K)
S_p	surface area in contact with plasma (cm²)
t	time (s)

T	temperature (K)
u_g	gas velocity in interwafer space (cm/s)
v_0	random thermal velocity of etchant species (cm/s)
V_p	volume occupied by the plasma (cm³)
w	wall recombination coefficient

Greek characters

α, β, γ	dimensionless groups defined in Eq. [8]
ζ	dimensionless radial position, r/R_o
η	effectiveness factor (Eq. [15])
σ	dimensionless film radius, R/R_o
τ	dimensionless time, $k_2c_0t/\chi h_o$
τ_0	dimensionless total etch time
ϕ	Thiele Modulus based on the film radius, $R(2k_2/LD)^{1/2}$
ϕ_o	Thiele Modulus based on the wafer radius, $R_o(2k_2/LD)^{1/2}$
χ	moles of A consumed per cm³ of film etched (mol/cm³)
ψ	dimensionless radial position, r/R

REFERENCES

1. S. M. Irving, *Solid State Technol.*, **14**, 47 (June 1971).
2. R. G. Poulsen, *J. Vac. Sci. Technol.*, **14**, 266 (1977).
3. R. D. Rust, R. J. Rhodes, and A. A. Parker, in "Plasma Processing," G. S. Mathad, G. C. Schwartz, and G. Smolinsky, Editors, p. 584, The Electrochemical Society Softbound Proceedings Series, Pennington, NJ (1983).
4. A. C. Adams, in "VLSI Technology," S. M. Sze, Editor, McGraw-Hill, New York (1983).
5. M. Doken and I. Miyata, *This Journal*, **126**, 2235 (1979).
6. J. F. Battey, *ibid.*, **124**, 437 (1977).
7. D. L. Flamm and V. M. Donnelly, *Plasma Chem. Plasma Proc.*, **1**, 317 (1981).
8. J. F. Battey, *This Journal*, **124**, 147 (1977).
9. J. C. Greaves and J. W. Linnett, *Trans. Faraday Soc.*, **55**, 1355 (1959).
10. C. J. Mogab, *This Journal*, **124**, 1262 (1977).
11. A. T. Bell, in "Techniques and Applications of Plasma Chemistry," J. R. Hollahan and A. T. Bell, Editors, John Wiley and Sons, New York (1974).
12. J. W. Coburn and M. Chen, *J. Vac. Sci. Technol.*, **18**, 3134 (1981).
13. A. Jacob, *Solid State Technol.*, 31 (June 1977).
14. P. C. Nordine and D. E. Rosner, *J. Chem. Soc. Faraday Trans.*, **72**, 1526 (1976).
15. A. Jacob, *Solid State Technol.*, 95 (April 1978).
16. A. A. Parker, R. J. Pachter, and R. D. Rust, in "Plasma Processing," G. S. Mathad, G. C. Schwartz, and G. Smolinsky, Editors, p. 596, The Electrochemical Society Softbound Proceedings Series, Pennington, NJ (1983).
17. E. E. Petersen, "Chemical Reaction Analysis," Prentice-Hall, Englewood Cliffs, NJ (1965).
18. K. F. Jensen and D. B. Graves, *This Journal*, **130**, 1950 (1983).
19. A. C. Lloyd, *Int. J. Chem. Kinetics*, **3**, 39 (1971).
20. D. L. Flamm, D. N. K. Wang, and D. Maydan, *This Journal*, **129**, 2755 (1982).
21. M. J. Kushner, *J. Appl. Phys.*, **53**, 2923 (1982).
22. M. J. Kushner, *ibid.*, **53**, 2939 (1982).
23. B. Chapman, "Glow Discharge Processes," p. 62, John Wiley and Sons, New York (1980).
24. B. S. Meyerson and W. Olbricht, *This Journal*, **131**, 2361 (1984).

Reaction Kinetics of Hg₁₋ₓCdₓTe/Br₂-CH₃OH

R. T. Talasek* and A. J. Syllaios*

Texas Instruments, Incorporated, Equipment Group, Dallas, Texas 75266

ABSTRACT

Bromine methanol solutions are extensively used in HgCdTe device processing technology. The relative reaction rates of Hg, Cd, and Te and HgCdTe with bromine in methanol have been studied. The reaction rate constants, reaction order, and some conclusions about the mechanisms of the reactions of the elements with bromine are reported here. The anisotropic nature of the reaction of the semiconductor with bromine has been demonstrated. The effects of mechanical action on the relative rates of the semiconductor constituents have been studied and are also discussed.

Mercury cadmium telluride is a semiconductor widely used in the fabrication of infrared detectors. Since it is a compound, HgCdTe is especially sensitive to chemical processing, and some processing may leave the semiconductor surface depleted of one or more elements. This depletion may affect the performance of devices dependent on the surface behavior of the semiconductor. One of these processes is the chemical etching or polishing of HgCdTe, which uses solutions of bromine in methanol. Electrolyte electroreflectance (EER) measurements indicate that the surface of HgCdTe is left tellurium rich after such chemical treatments (1). To study the chemistry of this polishing further, the chemical kinetics of the HgCdTe/Br₂-CH₃OH system were investigated by studying the reactions of the elements Hg, Cd, and Te and of HgCdTe with Br₂ in CH₃OH. The semiconductor reaction was studied under noncontact (etch) conditions and by making contact to a Pelon polishing pad.

The extent of a reaction in a kinetic study is generally monitored by some physical constant of the system proportional to the concentration of a particular component (2). In this case, the amount of product (metal in solution) was monitored by measuring the UV-visible absorption of metal ion complexes formed with diphenylthiocarbazone (dithizone) for Hg and Cd and with sodium diethyldithiocarbamate for Te (3-5). The reactions were quenched at various time intervals, rather than continuously moni-

*Electrochemical Society Active Member.

toring absorption, so that nothing was added to the etch solution that might affect the reaction.

For any physical measurement, λ (in this case, metal complex absorption) that is proportional to reaction extent, the following relation holds (2)

$$\frac{\lambda_\infty - \lambda}{\lambda_\infty - \lambda_0} = \frac{C}{C_0} \qquad [1]$$

where λ_∞ is the measurement at full extent of reaction, λ_0 the measurement at reaction initiation, λ the measurement at time t, C_0 the initial concentration of limiting reactant, and C the concentration of limiting reactant at time t.

Reactions of Hg, Cd, and Te with Br₂/CH₃OH

The following elemental oxidation reduction reactions were studied

$$Hg_{(l)} + Br_2(CH_3OH) \rightleftharpoons HgBr_2(CH_3OH)$$

$$Cd_{(s)} + Br_2(CH_3OH) \rightleftharpoons CdBr_2(CH_3OH)$$

$$Te_{(s)} + 2Br_2(CH_3OH) \rightleftharpoons TeBr_4(CH_3OH)$$
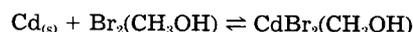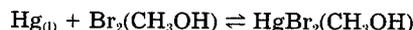
The reactions were studied by reacting the elemental metal with solutions of bromine in methanol in concentrations approximately equal to the effective metal concentration under convection-controlled conditions ($10^{-4}N$ > [Br₂] > $10^{-7}N$). For each reaction, a specific rate equa-